

SUCCESSFUL BEAM COMMISSIONING OF HEAVY-ION SUPERCONDUCTING LINAC AT RIKEN

K. Yamada*, T. Dantsuka, M. Fujimaki, E. Ikezawa, H. Imao, O. Kamigaito, M. Komiyama, K. Kumagai, T. Nagatomo, T. Nishi, H. Okuno, K. Ozeki, N. Sakamoto, K. Suda, A. Uchiyama, T. Watanabe, Y. Watanabe, RIKEN Nishina Center, Wako, Japan
E. Kako, H. Nakai, H. Sakai, K. Umemori, KEK, Tsukuba, Japan
H. Hara, A. Miyamoto, K. Sennyu, T. Yanagisawa,
Mitsubishi Heavy Industries Machinery Systems, Ltd. (MHI-MS), Kobe, Japan

Abstract

A new superconducting booster linac, called SRILAC, has been constructed at the RIKEN Nishina Center to upgrade the acceleration voltage of the existing linac to enable investigation of new super-heavy elements and production of useful radioactive isotopes. The SRILAC consists of 10 superconducting (SC) TEM quarter-wavelength resonators made from pure niobium sheets which operate at 4.5 K. We successfully developed high performance SC-cavities which satisfy the required Q_0 of 1×10^9 with a wide margin. Installation of the cryomodule and He refrigerator system was completed at the end of FY2018 and the first cooling test was performed in September 2019. After various preparations and tests, beam acceleration was successfully commissioned on January 28th, 2020. The project was successfully completed on schedule and the beam supply to experiments was started in June 2020. This paper reports on the beam commissioning of the SRILAC and the preparation and testing of the components for the commissioning.

INTRODUCTION

The RIKEN Nishina Center for Accelerator-Based Science promotes heavy-ion beam science through basic research, such as elucidating the origin of elements, and developing new nuclear models, synthesizing superheavy elements (SHEs) using high-intensity primary beams, by applying research such as nuclear transmutation, and industrial applications such as biological breeding and producing useful radio isotopes (RIs). The Radioactive Isotope Beam Factory (RIBF) [1, 2], the main facility at the RIKEN Nishina Center, started operation in 2006 and provides the world's most intense RI beam by accelerating heavy-ion beams with a cascade of four ring cyclotrons. Among them, the heavy-ion linac, RILAC, plays an important role as an injector for RIBF cyclotrons and also supplies a high intensity beam for SHE experiments and has been in operation since 1982. Figure 1(a) shows a schematic of the RILAC facility prior to 2017.

The RILAC was initially designed to have six drift-tube-linac (DTL) tanks with a total acceleration voltage of 16 MV [3]. Each DTL tank is a room-temperature (RT) quarter-wavelength resonator (QWR) which can vary its resonant frequency from 17 to 45 MHz in continuous wave

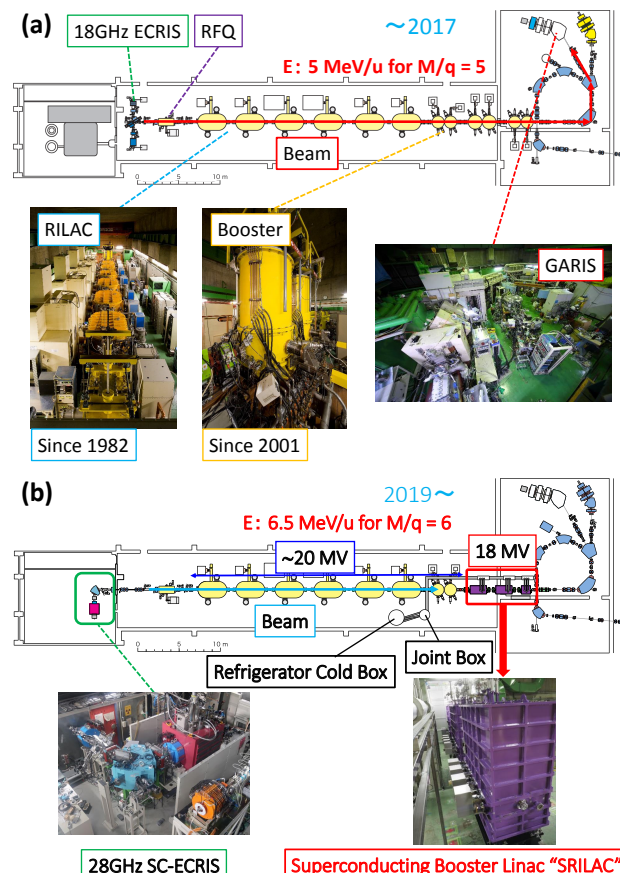


Figure 1: Schematic of the previous heavy-ion linac facility at RIKEN in 2017 (a) and the upgraded facility (b).

operation. In 1996, the front end of the RILAC, consisting of a combination of an 8 GHz electron-cyclotron-resonance ion source (ECRIS) and a 500 kV Cockcroft-Walton electrostatic accelerator was replaced with an 18 GHz ECRIS and a variable frequency RFQ linac [4] to increase the beam intensity. In order to increase the beam energy for SHE synthesis experiments, etc., six DTL cavities (A1–A6) with twice the resonant frequency of the RILAC were newly added downstream of the RILAC as a booster linac in 2001 [5]. The first two cavities, A1 and A2, have variable frequencies in the range 36–76.4 MHz, while the latter four cavities, A3–A6, have fixed frequencies of 75.5 MHz. With this modification, the RILAC was able to accelerate heavy ions with $m/q = 5$

* nari-yamada@riken.jp

to 5 MeV/u. Synthesis experiments on the 113th element [6] were performed using a $^{70}\text{Zn}^{14+}$ beam with an energy of 5 MeV/u accelerated by the RILAC and the booster with frequencies of 37.75 MHz and 75.5 MHz, respectively. The first synthesis of element 113 was achieved in July 2004, and the 113th element, nihonium, named for Japan, was listed in the periodic table in November 2016.

After the discovery of nihonium, we planned to use the RILAC to synthesize new SHEs above 119, as well as producing valuable RIs such as astatine. In particular, astatine is attracting attention for future medical applications such as cancer therapy. However, the existing RILAC could not provide the required beam energy for these purposes due to an insufficient acceleration voltage. Therefore, we decided [7] to build a new superconducting ECR ion source [8] to obtain a higher beam intensity, and to replace the four latter DTLs (A3–A6) with ten superconducting cavities to increase the beam energy, as shown in Fig. 1(b). The goal of the RI-LAC upgrade project is to be able to accelerate ions with $m/q = 6$ to 6.5 MeV/u. The budget was approved in fiscal 2016 and construction was completed in 2019. In this paper, we report an overview of the superconducting booster linac named SRILAC, the preparation and testing for the commissioning after the cryomodule (CM) installation, and the beam commissioning.

OVERVIEW OF SRILAC

General Layout and Cryomodule

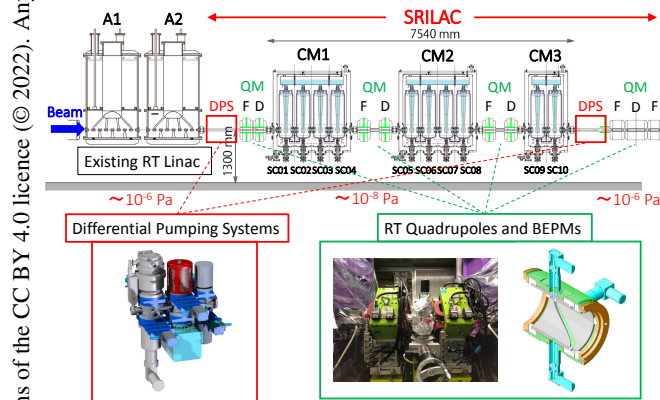


Figure 2: General layout of the SRILAC. F and D in the figure indicate the horizontal focusing polarity of the focusing element.

The general layout of the SRILAC [9] is shown in Fig. 2. The maximum-voltage-gain of the SRILAC was set to 18 MV in total to provide a margin in the beam energy. We fabricated ten superconducting quarter-wavelength resonators (SC-QWRs) to achieve the acceleration voltage in the limited space. The ten SC-QWRs (SC01–10) are arranged into groups of four units, four units, and two units, stored in three CMs (CM1–3) consisting of two full-size CMs and one half-size CM. The resonant frequency of the SC-QWR was set to be 73.0 MHz, which is the fourth harmonic of the

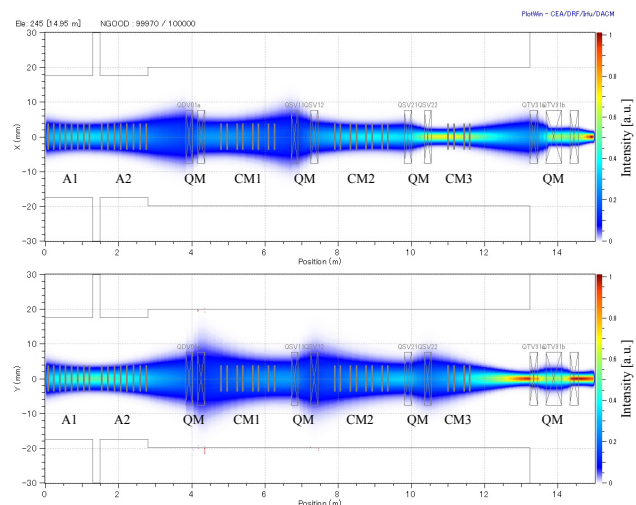


Figure 3: Example of the beam trajectory calculation for the SRILAC calculated by TraceWin code [10]. The beam emittance (6σ) was assumed to be 12.3 mm-mrad and 100 keV/u for the calculation.

fundamental frequency of the RIBF. The room-temperature quadrupole magnets (RT-QMs) are used as focusing elements of the SRILAC in order to simplify the structure of the CM. The maximum beam intensity is expected to be about $100 \mu\text{A}$ for SHE experiments. The SRILAC was designed to achieve a transmission efficiency of more than 99.9% for a beam current of $500 \mu\text{A}$ as a margin. An example beam trajectory calculation for the SRILAC is presented in Fig. 3. The example was calculated in the range shown in Fig. 2 for the case of accelerating $500 \mu\text{A}$ of ions with $m/q = 4$ up to 6.8 MeV/u .

To measure the beam position in the cold section, non-destructive beam monitors (BEPMs) were developed and installed [11] at each RT-QM between CMs and at the downstream of the SRILAC CM. The BEPM is based on a capacitive pickup with a pair of parabolic-cut electrodes. We can deduce the beam energy using the time-of-flight (TOF) between two BEPMs. An issue of concern in this project was that the CMs had to be connected to a very dirty beam-line that had been built decades ago. Since the vacuum of those beam-lines are of order 10^{-6} Pa, it is necessary to prevent gas flow from the beam-line. Therefore, we developed a three-stage differential pumping system (DPS) and installed it [12] on both sides of the cold section.

Figure 4 shows a schematic of a full-size CM for the SRI-LAC. The operation temperature of the CM is 4.5 K, using the liquid-helium refrigerator HELIAL MF manufactured by Air Liquide S.A. located in the vicinity of the CMs, as shown in Fig. 5. The vacuum vessel of the CM is made of carbon steel with electroless nickel plating to complement the shielding of the external magnetic field. The static heat load was estimated to be 18 W per full-size CM or 10 W per half-size CM. All the cold masses are mounted on the base plate by G10 pillars for thermal insulation, and the SC-QWRs are supported together at a point in consideration

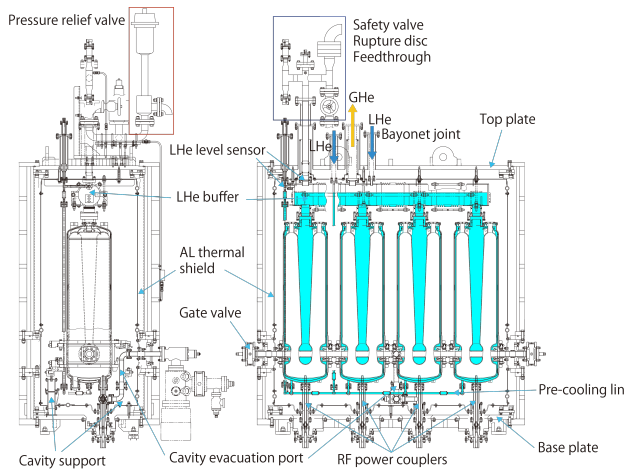


Figure 4: Schematic of a full-size CM for the SRILAC. Liquid helium is stored in the light blue area.

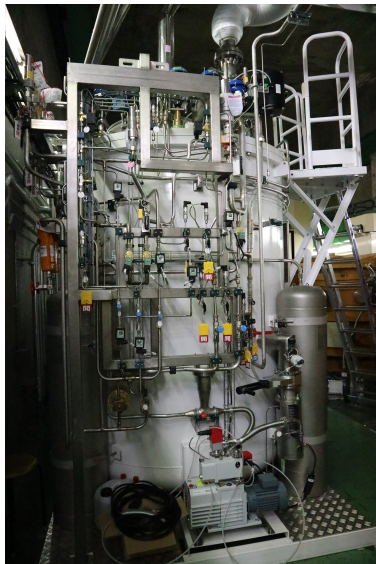


Figure 5: Cold box of the helium refrigerator for the SRILAC, HELIAL MF, manufactured by Air Liquide S.A.

of movement by heat contraction. A pressure relief valve is mounted on each CM to comply with the High Pressure Gas Safety Act in Japan. The CMs assembled at RIKEN were transported to the linac building and installed there at the end of the March 2019 [13]. The helium refrigeration system was also installed at about the same time. The design parameters of the SRILAC and its CM are summarized in Table 1.

Superconducting Acceleration Cavity

In the SC-QWR of the SRILAC, we adopted a conical shape for the stem to realize a better RF performance and robustness against mechanical vibration. The end face of the drift tube is cut at an angle to compensate for the beam deflection by the RF magnetic field. One prototype and ten actual cavities were fabricated using pure niobium sheets with a residual resistance ratio of 250 provided by Tokyo

Table 1: Design Parameters of the SRILAC (Upper Part) and its Cryomodule (Lower Part)

Number of CMs	3
Number of cavities	10
Frequency	73.0 MHz (c.w.)
E_{inj}	3.6 MeV/u
E_{ext} (tunable)	6.5 MeV/u for $m/q = 6$
Total acceleration voltage	18 MV (goal)
Operating temperature	4.5 K
Operating pressure	0.126 MPaA
Number of cavities per CM	4 or 2
Length (between GVs)	2200 or 1340 mm
Width	1060 mm
Total height with pedestal	3907 mm (incl. valves)
Cold focusing element	None
Material for vessel	Carbon steel with electroless nickel plating
Local magnetic shield	Permalloy 1.5 mm (inside the He jacket of each cavity)
Thermal shield temperature	80 K (LN ₂ cooling)
Static heat load	18 or 10 W to 4.5 K
Platform	Base plate
Cavity vacuum pump	IP + NEG(ZAO)
Insulation vacuum pump	TMP

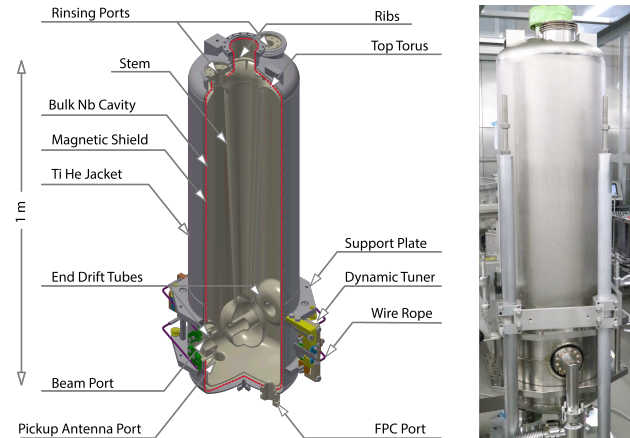


Figure 6: Schematic of a SC-QWR for the SRILAC (left) and a photo of one of the fabricated SC-QWRs (right).

Denkai Co. The surface treatment was performed based on buffered chemical polishing [14]. A helium jacket made of pure titanium was welded on the bulk SC-QWR. To reduce the complexity in assembling the CMs, a magnetic shield was installed between the bulk SC-QWR and the jacket. Figure 6 shows a schematic of an SC-QWR and a photo of one of the fabricated SC-QWRs with the jacket. The design parameters of the SC-QWRs are listed in Table 2. Details of the frequency adjustment during the SC-QWR fabrication are described in Ref. [15].

Table 2: Design Parameters of the SC-QWRs for the SRI-LAC; the surface resistance is conservatively assumed to be $22.4 \text{ n}\Omega$ in the calculation; the effective length for obtaining E_{acc} is set to $\beta_{\text{opt}}\lambda = 0.32 \text{ m}$

Frequency [MHz] at 4.5 K	73.0
Duty [%]	100
β_{opt}	0.078
Aperture [mm]	$\phi 40$
$G [\Omega]$	22.4
$R_{\text{sh}}/Q_0 [\Omega]$	579
Q_0	1.0×10^9
$P_0 [\text{W}]$	8
$V_{\text{acc}} [\text{MV}]$ at $E_{\text{acc}} = 6.8 \text{ MV/m}$, $\beta = 0.078$	2.2
$E_{\text{acc}} [\text{MV/m}]$	6.8
$E_{\text{peak}}/E_{\text{acc}}$	6.2
$B_{\text{peak}}/E_{\text{acc}}$ [mT/(MV/m)]	9.6

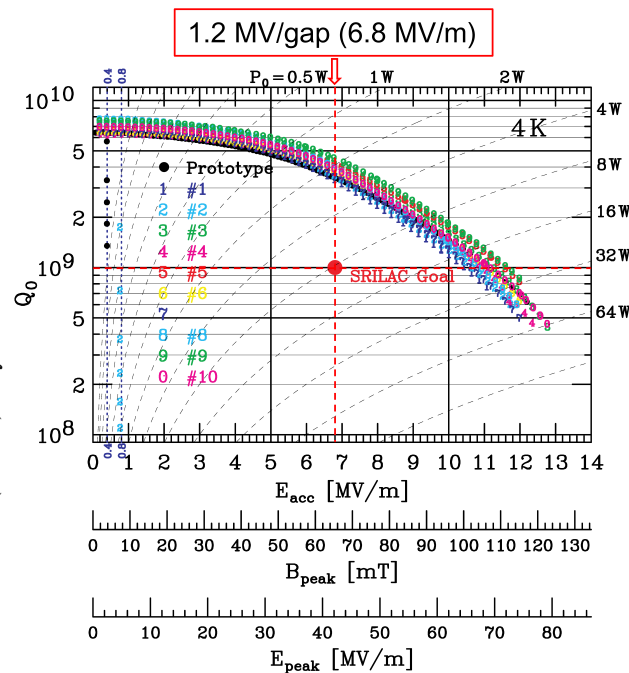


Figure 7: Q_0 vs E_{acc} plot of the bulk SC-QWRs measured at 4.2 K. The criteria of the SRILAC is $Q_0 = 1.0 \times 10^9$ at $E_{\text{acc}} = 6.8 \text{ MV/m}$.

All the SC-QWRs were fabricated by November 2018 and tested immediately. When the assembly of an SC-QWR was completed, a performance test was carried out sequentially at RIKEN to confirm whether acceptable performance was obtained. The details of the test procedure are the same as those given in Ref. [16]. Figure 7 shows the quality factor Q_0 plotted against acceleration voltage E_{acc} for all SC-QWRs. Although multipacting was observed at 0.9 MV/m for each SC-QWR in the figure, it could be processed within several hours. The test results indicate very high values of Q_0 and E_{acc} for all SC-QWRs fabricated; all the SC-QWRs exceeded the design goal. No exponential deterioration of Q_0 was

observed up to 12 MV/m for any of the SC-QWRs in the performance test.

PREPARATION AND TESTS FOR COMMISSIONING

Preparation of Equipment

As mentioned above, the three CMs were completed and installed by March 2019. After the installation of the CMs, a vacuum pumping system for the SC-QWRs was mounted on each CM in situ using local anti-static vinyl enclosures and ISO Class-1 clean bench Stand KOACH [17]. Then, the warm sections between each DPS and CM as well as between CMs were connected using the same system on site by the summer of 2019. A slow-leak and slow-pumping system using mass-flow controllers was introduced to the local clean work. Figure 8 shows the connection and installation of a warm section between CMs. First, a vacuum chamber was placed in the center between the CMs, and two vacuum pipes with one BEPM built-in were connected (Fig. 8(a)). After attaching vacuum pumps (we use an ion pump and a NEG pump) to the vacuum chamber (Fig. 8(b)), the two lower halves of the QMs were installed (Fig. 8(c)), and finally the upper halves were mounted on top to complete the process (Fig. 8(d)).

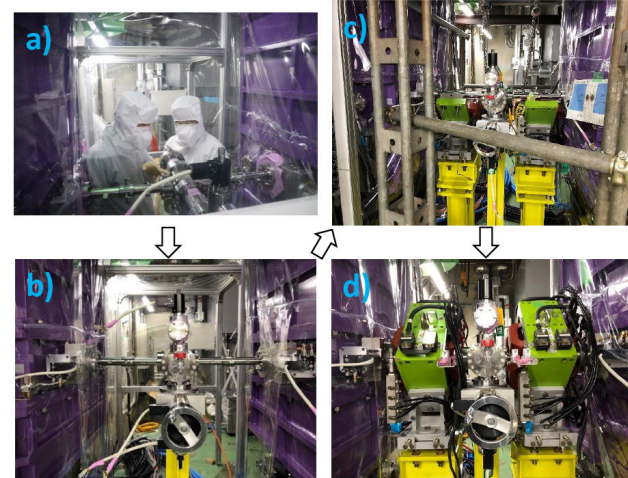


Figure 8: Connection and installation of a warm section between the SRILAC CMs.

In parallel, we installed the equipment control system for the CMs and RF system, connected their wirings, and set up the low-level RF circuits (LLRFs) and RF amplifiers by the fall of 2019. The control system based on a programmable logic controller is divided into two parts: one for the overall CM control and the other for the RF system control. The CM control system is equipped with a 30 kVA UPS, which includes the power supply for the vacuum pump. The digital LLRF of the SRILAC [18] is implemented in a XILINX XC6SLX150 FPGA with 4/5f sampling, and three AD9446 16-bit analog-to-digital converters and an AD9557BSVZ direct digital synthesizer are used in the circuit. A solid

state amplifier for each SC-QWR has built-in isolators and maximum output powers of 7.5 kW in c.w., which enables an operational bandwidth of ± 50 Hz.

Cryomodule Cooling Test

The first cooling test of CMs was conducted in September 2019 after the completion of the CM control system. Temperature curves of each CM during the cooling test are shown in Fig. 9. The CMs were successfully cooled down without any serious trouble. The temperature drop just after the start of cooling is thought to be due to the fact that the inside of the refrigerator was still partially cool from the refrigerator unit test. This phenomenon did not occur during the subsequent cooling. The cooling stagnation seen at about 120 K was caused by a minor vacuum leak in the cold box of the refrigerator. The leak was not in the cold box itself, but in the ISO-KF25 tee of the vacuum pumping system. The cooling down time from room temperature was found to be about 3.5 days to fill up with liquid helium. Note that the helium refrigerator of the SRILAC has a cooling capacity of over 700 W at 4.5 K.

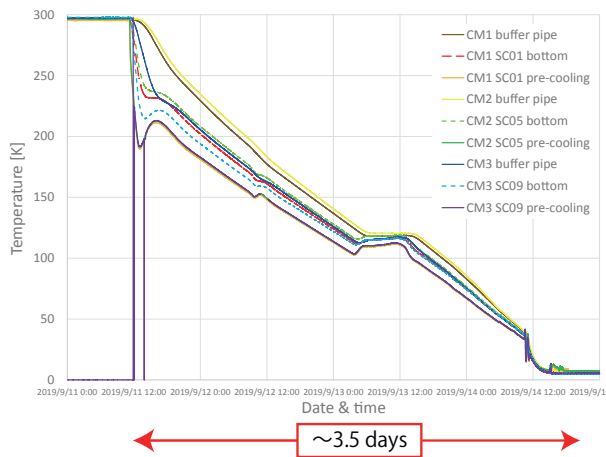


Figure 9: Temperature curve during the first cooling down of the SRILAC CMs. The temperatures of the liquid helium buffer, bottom of the upstream SC-QWR, and the pre-cooler line are plotted for each CM.

However, during the warm-up process after the four cooling down, a vacuum leak occurred from the fundamental power coupler of SC05 on November 2019. This was before the high power RF test was performed. Therefore the SC05 could not be used for the hardware tests and beam commissioning. Subsequently, a vacuum leak occurred from the coupler of SC06 on October 2020 during beam delivery after beam commissioning. These coupler issues will be detailed at the end of this paper.

Figure 10 shows a one-day trend of the helium pressure and the opening of the helium-gas return valve of each CM. The lower part shows the helium pressure and the upper part shows the valve opening. In this trend, the RF was actually excited on the SC-QWR and the CMs were heat loaded. As shown in the figure, the absolute pressure of the helium was

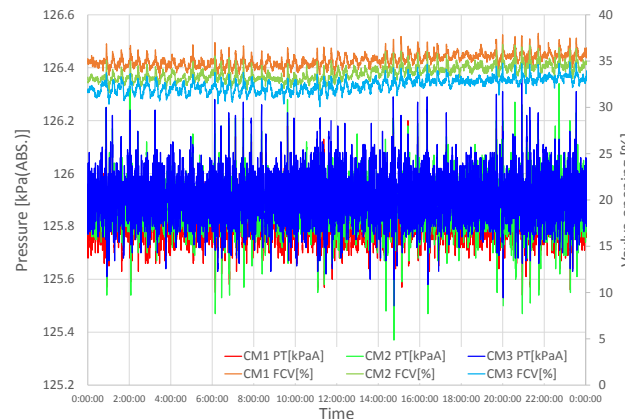


Figure 10: One-day trend of the helium pressure and gas return valve opening of each CM.

well stabilized within ± 0.4 kPa by controlling the gas return valve. Since the frequency sensitivity to the pressure variation $\Delta f / \Delta P_{\text{He}}$ is -2.0 Hz/hPa for the SRILAC SC-QWR, the pressure fluctuation corresponds to the resonant frequency variation of ± 8 Hz, which is considerably smaller than the operational bandwidth. Thus, the SRILAC SC-QWR can be operated by simply compensating with a slow tuner.

High Power RF Test

After the LLRFs, RF amplifiers, and RF control system were ready, we performed high power RF tests on nine SC-QWRs, excluding SC05. We took a few days to overcome the multipacting of all nine SC-QWRs. Then, the RF feedback parameters on the LLRFs were tuned to compensate the effect of microphonics. Power spectra of the cavity pickup

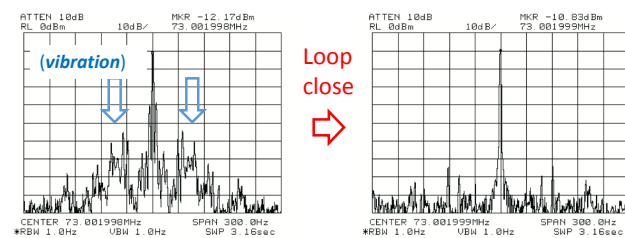


Figure 11: Power spectra of the cavity pickup signal for the case of open (left) and closed (right) feedback loops.

The X-ray emission was measured at each voltage before opening the gate valves [19]. Unfortunately, field emissions were observed in some SC-QWRs, especially in CM2. CM1, the last to be assembled, was the cleanest. The evolution of the field emission is also described in Ref. [19].

Frequency tuning of the SC-QWRs was realized by compressing the beam ports in the direction of the beam axis [18]. The frequency is lowered by pressing both beam ports to the cavity-center using metallic wires pulled by a stepping

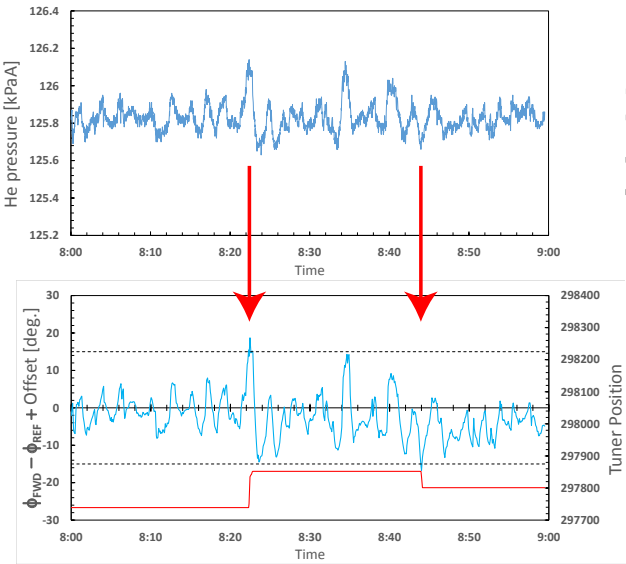


Figure 12: Automatic frequency compensation by the tuner when the phase difference exceeded the dead zone.

motor placed out of the CM. The tuner can be adjusted to -14 kHz with a sensitivity of 19 kHz per millimeter. The frequency variation due to the helium pressure fluctuation is automatically compensated by proportional control of the tuner. The tuner is driven by the phase difference between the forward and reflection signals on a directional coupler. The compensation by the tuner is shown in Fig. 12. As can be seen in the figure, the tuner moved to compensate for the frequency when the phase difference exceeded the dead zone of 15 degrees.

Effect of DPS

As mentioned above, the vacuum level difference was about 10^2 order between the cold section and the beam line at each end of the cold section. In addition, for the SHE experiments, the user group uses 0.55 Torr helium gas in the Gas-filled Recoil Ion Separator (GARIS3) in performing the measurement. Although a differential pumping system is also installed in front of the user target, it is not enough to block the helium gas on the cold section. When the GARIS3 was filled with helium gas, the vacuum level of each position in the beam line deteriorated as shown in Fig. 13. However, the influence on the cold section was well suppressed by the DPS installed at each end of the cold section. The CMs can be operated stably with almost no influence from the dirty beam lines at both ends due to the DPS [19].

BEAM COMMISSIONING

After the preparation and tests were completed, we performed a beam acceleration test using the RT linac part without the RF voltage of the SRILAC. An acceleration beam of ${}^{40}\text{Ar}^{13+}$ was selected, according to the user's request. The beam emittance can be defined using three sets of beam slits installed in the low-energy beam transport (LEBT) between the ion source and the RFQ. For this test, the beam

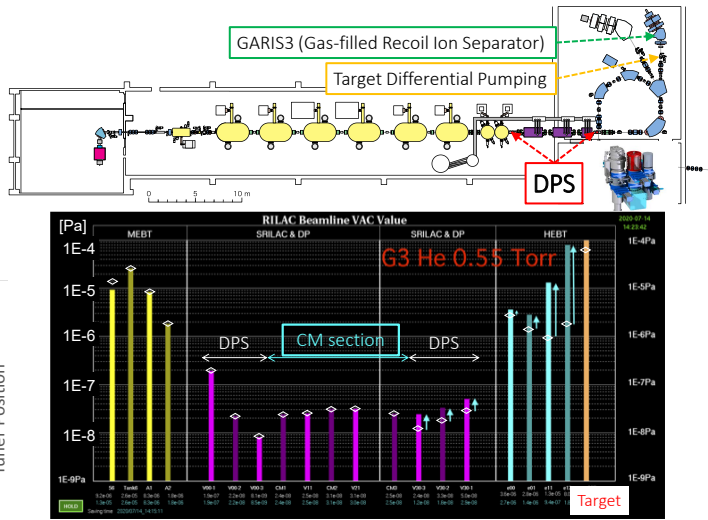


Figure 13: Change in the beam-line vacuum level when the GARIS3 was filled with 0.55 Torr helium gas. The white diamonds in the figure indicate the vacuum level before filling with helium gas. All the gate valves were opened at this time.

emittance (4σ) was set to be about $12 \text{ mm}\cdot\text{mrad}$ horizontal and $6 \text{ mm}\cdot\text{mrad}$ vertical at the LEBT. The RT linac part was carefully adjusted while the energy was measured using the TOF signal of the BEPMs.

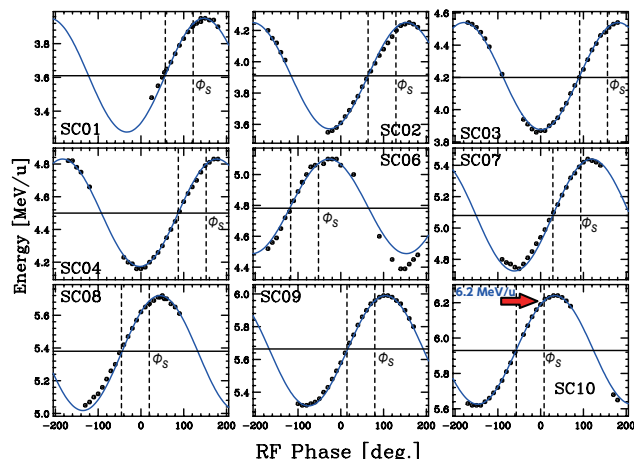


Figure 14: Beam energies measured at different RF phases for each SC-QWR plotted against the RF phase.

After the specified energy and sufficient transmission efficiency were obtained, we started beam acceleration by the SRILAC except for SC05 on the morning of January 28th, 2020. By exciting the cavities one by one and changing the RF phase for each cavity as shown in Fig. 14, the synchronous phase was determined to be the designed value for each SC-QWR. Then, the RF voltage was adjusted to match the specified beam energy for each SC-QWR. Finally, the beam energy reached the commissioning goal of 6.2 MeV/u at around 9 p.m. on the same day, as shown in Fig. 15.



Figure 15: Measurement screen of the BEPM system (preliminary version). The specified energy of 6.2 MeV/u was obtained.



Figure 16: Fluorescence produced by the high intensity ^{40}Ar beam during an SHE experiment.

The absolute value of the gap voltage of each SC-QWR was also corrected by the energy measurement. In a subsequent acceleration test, the beam profile was measured using two wire scanners located downstream of the SRILAC. The phase space plot was deduced by measuring the beam spread with ten different optics parameters and fitting it with the calculation. The results show there was no obvious emittance growth in the SRILAC part, although a slight problem in the RT linac part was observed.

After the successful first beam acceleration of the SRILAC, we passed the facility inspection by the Nuclear Regulation Authority at the end of fiscal year 2019. The project was successfully completed on schedule. We started supplying beams to the SHE research from June 2020. The fluorescence produced by the high intensity ^{40}Ar beam is

shown in Fig. 16. We are currently supplying a $^{51}\text{V}^{13+}$ beam for an SHE experiment.

ISSUE AND OUTLOOK

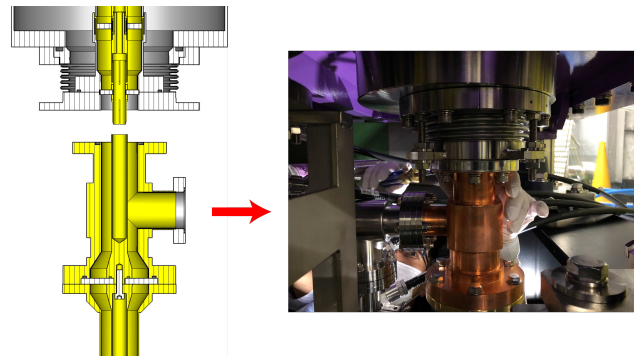


Figure 17: Schematic of an outer window (left) and a photo of the SC06 coupler being installed.

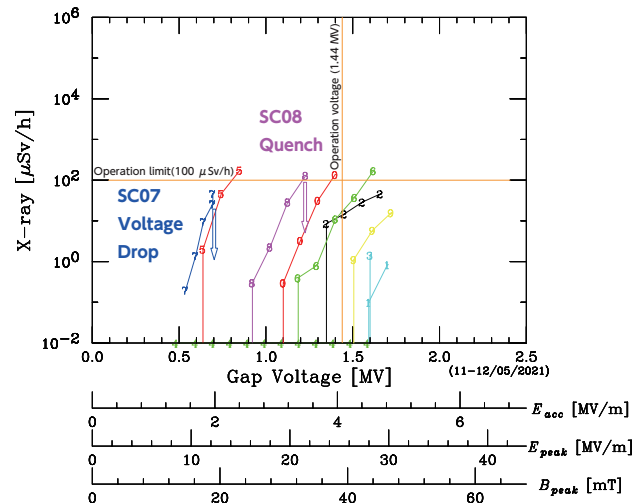


Figure 18: Radiation levels of x-rays for each SC-QWR plotted against gap voltage.

The SRILAC has been operating smoothly to date, except for the coupler issue of CM2. After the second vacuum leak occurred from the SC06 coupler in October 2020, we inspected the inner surface of each coupler with an endoscope [20]. Although the SRILAC couplers were designed as a single RT window type, the inside of all the couplers were rusted due to condensation. The ceramic window was set slightly inside the CM and was designed for low heat transfer, so the windows seemed to cool down. Galvanic corrosion may have affected the metalization of the window ceramics, which may have caused the vacuum leak. To prevent further damage to the remaining eight couplers, we immediately took measures to flow dry nitrogen through the inside of the couplers. Ten new couplers with countermeasures are also being manufactured.

In order to tentatively recover SC05 and SC06, we made and mounted an outer window as shown in Fig. 17 for the

couplers of SC05 and SC06 in April 2021. The inside of the attached outer window is evacuated with a TMP. Figure 18 shows measurements of X-rays after mounting the outer window. We succeeded in reviving SC05 and SC06 at a slightly lower voltage, although SC07 and SC08 have been contaminated by repeated vacuum leaks.

We plan to attach outer windows on the remaining eight couplers this summer. To allow the SHE experiments to continue, we will operate the SRILAC in its current state for the time being. The replacements of the couplers will be done after careful consideration of the replacement method. Eventually, we hope to re-clean the SC-QWR of CM2 to recover its performance.

ACKNOWLEDGEMENTS

The authors are grateful to Prof. K. Saito at FRIB/MSU for technical advice on the design of the cavity and assembly work. We would like to thank Prof. T. Toyama at KEK/J-PARC for calibrating and mapping the BEPMs. We would like to express our gratitude to the operators from SHI Accelerator Services for their hard work from preparation to beam operation.

REFERENCES

- [1] Y. Yano, “The RIKEN RI Beam Factory Project: A status report,’ *Nucl. Instr. Meth. B*, vol. 261, pp. 1009-1013, 2007. doi:10.1016/j.nimb.2007.04.174
- [2] H. Okuno *et al.*, “Progress of RIBF accelerators,” *Prog. Theor. Exp. Phys.*, vol. 2012, p. 03C002, 2012. doi:10.1093/ptep/pts046
- [3] M. Odera *et al.*, “Variable frequency heavy-ion linac, RILAC: I. Design, construction and operation of its accelerating structure.” *Nucl. Instr. Meth. A*, vol. 227, no. 2, pp. 187-195, 1984. doi:10.1016/0168-9002(84)90121-9
- [4] O. Kamigaito *et al.*, “Construction of a variable-frequency radio-frequency quadrupole linac for the RIKEN heavy-ion linac,” *Rev. Sci. Instr.*, vol. 70, p. 4523-4531, 1999. doi:10.1063/1.1150105
- [5] O. Kamigaito *et al.*, “Construction of a booster linac for the RIKEN heavy-ion linac,” *Rev. Sci. Instr.*, vol. 76, p. 013306, 2005. doi:10.1063/1.1834708
- [6] K. Morita *et al.*, “New Result in the Production and Decay of an Isotope, 278113, of the 113th Element,” *J. Phys. Soc. Jpn.*, vol. 81, p. 103201, 2012. doi:10.1143/JPSJ.81.103201
- [7] O. Kamigaito *et al.*, “Present Status and Future Plan of RIKEN RI Beam Factory”, in *Proc. 7th Int. Particle Accelerator Conf. (IPAC'16)*, Busan, Korea, May 2016, pp. 1281-1283. doi:10.18429/JACoW-IPAC2016-TUPMR022
- [8] T. Nagatomo *et al.*, “New 28-GHz Superconducting ECR Ion Source for Synthesizing New Super Heavy Elements of Z > 118”, in *Proc. 23th International Workshop on ECR Ion Sources (ECRIS'18)*, Catania, Italy, Sep. 2018, pp. 53–57. doi:10.18429/JACoW-ECRIS2018-TUA3
- [9] N. Sakamoto *et al.*, “Construction Status of the Superconducting Linac at RIKEN RIBF”, in *Proc. 29th Linear Accelerator Conf. (LINAC'18)*, Beijing, China, Sep. 2018, pp. 620–625. doi:10.18429/JACoW-LINAC2018-WE2A03
- [10] D. Uriot and N. Pichoff, “Status of TraceWin Code”, in *Proc. 6th Int. Particle Accelerator Conf. (IPAC'15)*, Richmond, VA, USA, May 2015, pp. 92–94. doi:10.18429/JACoW-IPAC2015-MOPWA008
- [11] T. Watanabe *et al.*, “Commissioning of the Beam Energy Position Monitor System for the Superconducting RIKEN Heavy-ion Linac”, in *Proc. 9th Int. Beam Instrumentation Conf. (IBIC'20)*, Santos, Brazil, Sep. 2020, pp. 295–302. doi:10.18429/JACoW-IBIC2020-FRA004
- [12] H. Imao *et al.*, “Non-Evaporative Getter-Based Differential Pumping System for SRILAC at RIBF”, in *Proc. 19th Int. Conf. RF Superconductivity (SRF'19)*, Dresden, Germany, Jun.-Jul. 2019, pp. 419–423. doi:10.18429/JACoW-SRF2019-TUP013
- [13] K. Yamada *et al.*, “Construction of Superconducting Linac Booster for Heavy-Ion Linac at RIKEN Nishina Center”, in *Proc. 19th Int. Conf. RF Superconductivity (SRF'19)*, Dresden, Germany, Jun.-Jul. 2019, pp. 502–507. doi:10.18429/JACoW-SRF2019-TUP037
- [14] A. Miyamoto, H. Hara, K. Kanaoka, K. Okihira, K. Sennyu, and T. Yanagisawa, “MHI’s Production Activities of Superconducting Cavity”, in *Proc. 17th Int. Conf. RF Superconductivity (SRF'15)*, Whistler, Canada, Sep. 2015, pp. 1141–1145. doi:10.18429/JACoW-SRF2015-THPB029
- [15] K. Suda *et al.*, “Fabrication and Performance of Superconducting Quarter-Wavelength Resonators for SRILAC”, in *Proc. 19th Int. Conf. RF Superconductivity (SRF'19)*, Dresden, Germany, Jun.-Jul. 2019, pp. 182–187. doi:10.18429/JACoW-SRF2019-MOP055
- [16] K. Yamada *et al.*, “First Vertical Test of Superconducting QWR Prototype at RIKEN”, in *Proc. 28th Linear Accelerator Conf. (LINAC'16)*, East Lansing, MI, USA, Sep. 2016, pp. 939–942. doi:10.18429/JACoW-LINAC2016-THPLR040
- [17] https://www.koken-ltd.co.jp/english/koach/introduction/koach_c900-f_c645-f.html
- [18] K. Suda *et al.*, “New Frequency-Tuning System and Digital LLRF for Stable and Reliable Operation of SRILAC,” presented at SRF’2021, Grand Rapids, MI, USA, paper WEPTEV013, this conference.
- [19] N. Sakamoto *et al.*, “Operation Experience of the Superconducting Linac at RIKEN RIBF,” presented at SRF’2021, Grand Rapids, MI, USA, paper MOPFAV005, this conference.
- [20] K. Ozeki *et al.*, “FPC for RIKEN QWR,” presented at SRF’2021, Grand Rapids, MI, USA, paper THPTEV001, this conference.